Robotica (2005) volume 23, pp. 595–606. © 2005 Cambridge University Press
doi:10.1017/S0263574704001195 Printed in the United Kingdom

Modelling and simulation of artificial locomotion systems

Manuel F. Silva*, J. A. Tenreiro Machado and António M. Lopes†

(Received in Final Form: October 8, 2004)

SUMMARY

This paper describes a simulation model for a multi-legged locomotion system with joints at the legs having viscous friction, flexibility and backlash. For that objective the robot prescribed motion is characterized in terms of several locomotion variables. Moreover, the robot body is divided into several segments in order to emulate the behaviour of an animal spine. The foot-ground interaction is modelled through a non-linear spring-dashpot system whose parameters are extracted from the studies on soil mechanics. To conclude, the performance of the developed simulation model is evaluated through a set of experiments while the robot leg joints are controlled using fractional order algorithms.

KEYWORDS: Robotics; Walking; Dynamic modelling; Kinematics; Simulation; Saturation; Friction; Backlash; Fractional calculus.

I. INTRODUCTION

Walking machines allow locomotion in terrain inaccessible to other type of vehicles, since they do not need a continuous support surface.[1] On the other hand, the requirements for leg coordination and control impose difficulties beyond those encountered in wheeled robots.[2] These aspects deserve great interest and, in order to study them, different approaches may be adopted. One possibility is to design and build a walking robot and develop study based on the prototype. An alternative perspective consists on the development of simulation models of walking machines that serve as the basis for the research. This second approach has several advantages, namely lower development costs and a smaller time for implementing the modifications. Due to these reasons, several different simulation models were developed, and are used for the study, design, optimization, gait analysis and development of control algorithms.

The gait analysis and selection is a research area requiring an appreciable modelling effort for the improvement of mobility with legs in unstructured environments. Several articles addressed the structure and selection of locomotion modes.[3,4] Nevertheless, there are different optimization criteria such as energy efficiency,[5] stability,[4] velocity [6,7] and mobility.[8]

With respect to the control of legged robots, there exist a class of walking machines for which locomotion is a natural dynamic mode. Once started on a shallow slope, a machine of this class will settle into a steady gait, without active control or energy input.[9,10] However, the capabilities of these machines are quite limited. Previous studies focused mainly in the control at the leg level and leg coordination using neural networks,[11] fuzzy logic,[12] central pattern generators,[13] subsumption architecture[14] and virtual model control.[15] There is also a growing interest in using insect locomotion schemes to control walking robots. In spite of the diversity of approaches, for multi-legged robots the control at the joint level is usually implemented through a simple *PID* like scheme with position/velocity feedback. Other approaches include sliding mode control,[16] computed torque control[17] and hybrid force/position control.[18]

In this line of thought, this paper presents a simulation model for multi-leg locomotion systems and several periodic gaits. This tool is the basis for the study of the best system configuration and the type of movements that lead to a better mechanical implementation.[19–21] Moreover, the model is also used to study the control, at the joint leg level, in the presence of joints with viscous friction, flexibility and backlash.[22,23]

Bearing these facts in mind, the paper is organized as follows: Section two introduces the robot kinematic model and the motion planning scheme. Sections three and four present the robot dynamic model and the foot-ground interaction model. Section five develops a set of experiments to evaluate the system performance under Fractional Order (*FO*) joint leg control. Finally, section six outlines the main conclusions.

II. ROBOT KINEMATIC MODEL

We consider a walking system (Figure 1) with n legs, equally distributed along both sides of the robot body, having each two degrees of freedom (*dof*) corresponding to two rotational joints (*i.e.* $j = \{1, 2\} \equiv \{\text{hip, knee}\}$).

Motion is described by means of a world coordinate system. The kinematic model comprises: the cycle time T, the duty factor β, the transference time $t_T = (1 - \beta)T$, the support time $t_S = \beta T$, the step length L_S, the stroke pitch S_P, the body height H_B, the maximum foot clearance F_C, the ith leg lengths L_{i1} and L_{i2} and the foot trajectory offset O_i $(i = 1, \ldots, n)$. Moreover, we consider a periodic trajectory for each foot, with constant body velocity $V_F = L_S/T$.

Gaits describe discontinuous sequences of leg movements, alternating between transfer and support phases and, in the

Corresponding Author: Prof. Manuel F. Silva.
E-mail: mfsilva@dee.isep.ipp.pt
* Department of Electrical Engineering, Institute of Engineering of Porto, 4200-072 Porto, (Portugal). E-mail: {mfsilva,jtm}@dee.isep.ipp.pt
† Department of Mechanical Engineering, Faculty of Engineering of Porto, 4200-465 Porto, (Portugal). E-mail: aml@fe.up.pt

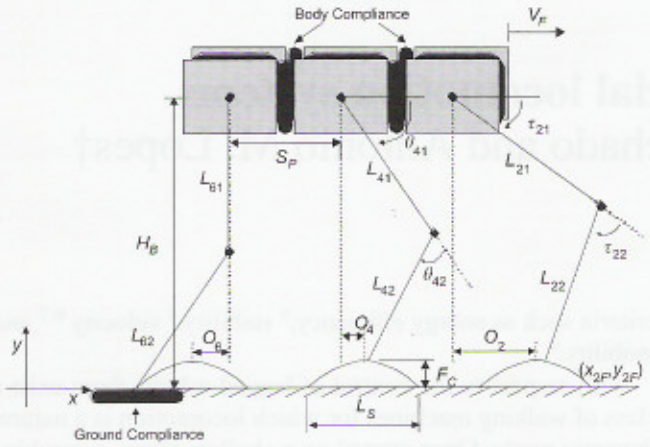

Fig. 1. Kinematic and dynamic multi-legged robot model.

simulation model, we consider the Wave gait, Equal Phase Half Cycle gait, Equal Phase Full Cycle gait, Backward Wave gait, Backward Equal Phase Half Cycle gait and Backward Equal Phase Full Cycle gait $\{WG, EPHC, EPFC, BW, BEPHC, BEPFC\}$.[2] Given a particular gait and duty factor β, it is possible to calculate, for leg i, the corresponding phase ϕ_i, the time instant where each leg leaves and returns to contact with the ground and the Cartesian trajectories of the tip of the feet (that must be completed during t_T).[2] Based on this data, the trajectory generator is responsible for producing a motion that synchronises and coordinates the legs.

Concerning the movement of the tip of the feet during the transfer phase, the trajectories must be performed in such a way to avoid collisions with ground or any obstacles that may be in the vicinity of the robot. This problem is more acute when the robot is walking with a periodic gait because, during the locomotion in irregular terrains, where it may be necessary to adopt a non-periodic locomotion gait, the trajectory of each robot feet might have to be distinct of each other.

To solve this problem several different strategies have been proposed. The following sub-section describes several foot trajectory planning schemes. Based on those studies, in sub-section II.2, it is presented the adopted solution, while detailing the entire robot locomotion planning process.

II.1. Transfer phase feet trajectory planning

When the robot design is a mimic of an animal, a frequently adopted approach consists on copying the animal feet trajectories. These animals are often filmed with special techniques, while walking on a treadmill, and the resulting film is analyzed to extract their feet trajectories in order to implement similar ones in the walking machines. Examples of this approach are the works of Bai *et al.* on the study of the cockroach,[24] Villanova *et al.* on the study of the hedgehog,[25] and Laksanacharoen *et al.* on the study of the cricket.[26]

A slightly different approach has been adopted by Pfeiffer *et al.*.[27] The study of the stick-insect is the base for implementing the feet trajectories of the TUM walking hexapod. However, on this case, the knee and the ankle joint leg coordinates are a mathematical function of the value of the hip joint coordinate. It was shown that the resulting trajectories are very close to the ones observed in insects during their locomotion.

Another strategy, often adopted, considers that the robot feet trajectories, in the Cartesian space, are mathematical functions based on the sine and cosine functions[28–30] or combinations of these.[31] Different mathematical formulae, such as circle arcs,[32] ovals,[33] ellipsis [30] and cycloidal functions [34] have also been adopted. Alternatively, Koyachi *et al.* adopt a spline to describe the feet trajectory during the transfer phase.[35] Jiménez and Santos established a rectangular trajectory during the feet transfer phase, either in the world or on the robot coordinate system, for the Rimho quadruped robot.[36] According to them, the rectangular trajectory in the world coordinate system presents the disadvantage of not being able to avoid collisions with the terrain, since the feet do not present a vertical movement during the lift-off and return to contact with the ground.

The trajectory of feet transfer phase can also be defined based on the optimization of mathematical indices.[37,38] Finally, Chevallereau *et al.* established ballistic dynamics during the transfer phase (*i.e.* no torque applied to the leg actuators during this period) to define the reference trajectories of a quadruped robot.[39]

II.2. Robot trajectory planning

Motivated by the above described methods, on a previous work we evaluated two alternative space-time foot trajectories, namely a cycloidal function (1a) where the feet lift-off and return to contact with the ground is vertical and a sinusoidal function (1b) where the trajectory is horizontal at those locations.[23] For example, considering that the transfer phase starts at $t=0$ for leg $i=1$ we have for $\mathbf{p_{Fd}}(t)=[x_{iFd}(t),\ y_{iFd}(t)]^{\mathrm{T}}$:

- during the transfer phase:

$$\mathbf{P_{Fd}}(t)=\begin{bmatrix} V_F\left[t-\dfrac{T}{2\pi}\sin\left(\dfrac{2\pi t}{T}\right)\right] \\ \dfrac{F_C}{2}\left[1-\cos\left(\dfrac{2\pi t}{T}\right)\right]\end{bmatrix} \tag{1a}$$

$$\mathbf{P_{Fd}}(t)=\begin{bmatrix} \left(\dfrac{t_T}{T}\right)\left[\left(\dfrac{L_s t}{t_T}\right)-\dfrac{L_s}{2\pi}\sin\left(\dfrac{2\pi t}{T}\right)\right] \\ \dfrac{2F_C t'}{T}-\dfrac{F_C}{2\pi}\sin\left(\dfrac{4\pi t'}{T}\right)\end{bmatrix},$$

$$t'=\begin{cases} t, & 0\le t<T/2 \\ T-t, & T/2\le t<T\end{cases} \tag{1b}$$

- during the stance phase:

$$\mathbf{P_{Fd}}(t)=[V_F T \quad 0]^{\mathrm{T}} \tag{2}$$

It was demonstrated that the cycloid is superior to the sinusoidal function, because it improves the hip and foot trajectory tracking, while minimising the corresponding joint torques.[23] For different acceleration profiles of the foot trajectory there were no significant changes of these results.

From the studies in biomechanics, Hodgins concludes that the disturbances that occur at the instants of feet impact

with the ground can be diminished by lowering the relative speed of the feet and the ground at the contact time.[40] This technique, often called ground speed matching, appears to justify the reason why the feet cycloidal trajectory is superior to the sinusoidal one.

The robot body, and by consequence the legs hips, is assumed to have a desired horizontal movement with a constant forward speed V_F. Therefore, for leg i the Cartesian coordinates of the hip of the legs are given by $\mathbf{p_{Hd}}(t) = [x_{iHd}(t), y_{iHd}(t)]^{\mathrm{T}}$:

$$\mathbf{P_{Hd}}(t) = [V_F t \quad H_B]^{\mathrm{T}} \tag{3}$$

The algorithm for the forward motion planning accepts the desired cartesian trajectories of the leg feet $\mathbf{p_{Fd}}(t)$ and hips $\mathbf{p_{Hd}}(t)$ as inputs and, by means of an inverse kinematics algorithm Ψ^{-1}, generates the related joint trajectories $\mathbf{\Theta_d}(t) = [\theta_{i1d}(t), \theta_{i2d}(t)]^{\mathrm{T}}$, selecting the solution corresponding to a forward knee:

$$\mathbf{P_d}(t) = [x_{id}(t) \quad y_{id}(t)]^{\mathrm{T}} = \mathbf{P_{Hd}}(t) - \mathbf{P_{Fd}}(t) \tag{4a}$$

$$\mathbf{P_d}(t) = \Psi[\mathbf{\Theta_d}(t)] \Rightarrow \mathbf{\Theta_d}(t) = \Psi^{-1}[\mathbf{P_d}(t)] \tag{4b}$$

$$\dot{\mathbf{\Theta}}_{\mathbf{d}}(t) = \mathbf{J}^{-1}[\dot{\mathbf{P}}_{\mathbf{d}}(t)], \mathbf{J} = \frac{\partial \Psi}{\partial \mathbf{\Theta}} \tag{4c}$$

To avoid the impact and friction effects, at the planning phase we estimate null velocities of the feet in the instants of landing and taking off, assuring also the velocity continuity.

III. ROBOT DYNAMICAL MODEL

III.1. Inverse dynamics computation

In order to derive the inverse dynamic equations of the multi-legged locomotion robot we adopt the Lagrange method ((5a) and (5b)):

$$\mathbf{L} = \mathbf{K} - \mathbf{U} \tag{5a}$$

$$\mathbf{\Gamma} = \frac{d}{dt}\left(\frac{\partial \mathbf{L}}{\partial \dot{\mathbf{\Theta}}}\right) - \frac{\partial \mathbf{L}}{\partial \mathbf{\Theta}} \tag{5b}$$

This formalism requires the calculation of the potential and kinetic energies, both for the body, the links and the feet of all robot legs. Other alternative derivation methods, for yielding the robot inverse dynamics, are described by different authors.[17,41–44]

The model for the robot inverse dynamics is formulated as:

$$\mathbf{\Gamma} = \mathbf{H}(\mathbf{\Theta})\ddot{\mathbf{\Theta}} + \mathbf{c}(\mathbf{\Theta}, \dot{\mathbf{\Theta}}) + \mathbf{g}(\mathbf{\Theta}) - \mathbf{F_{RH}} - \mathbf{J_F^T}(\mathbf{\Theta})\mathbf{F_{RF}} \tag{6}$$

where $\mathbf{\Gamma} = [f_{ixH}, f_{iyH}, \tau_{i1}, \tau_{i2}]^{\mathrm{T}} (i = 1, \ldots, n)$ is the vector of forces/torques, $\mathbf{\Theta} = [x_{iH}, y_{iH}, \theta_{i1}, \theta_{i2}]^{\mathrm{T}}$ is the vector of position coordinates, $\mathbf{H}(\mathbf{\Theta})$ is the inertia matrix and $\mathbf{c}(\mathbf{\Theta}, \dot{\mathbf{\Theta}})$ and $\mathbf{g}(\mathbf{\Theta})$ are the vectors of centrifugal/Coriolis and gravitational forces/torques, respectively. The $n \times m$ matrix $\mathbf{J_F^T}(\mathbf{\Theta})$ is the transpose of the robot Jacobian matrix, $\mathbf{F_{RH}}$ is the $m \times 1$ vector of the body inter-segment forces and

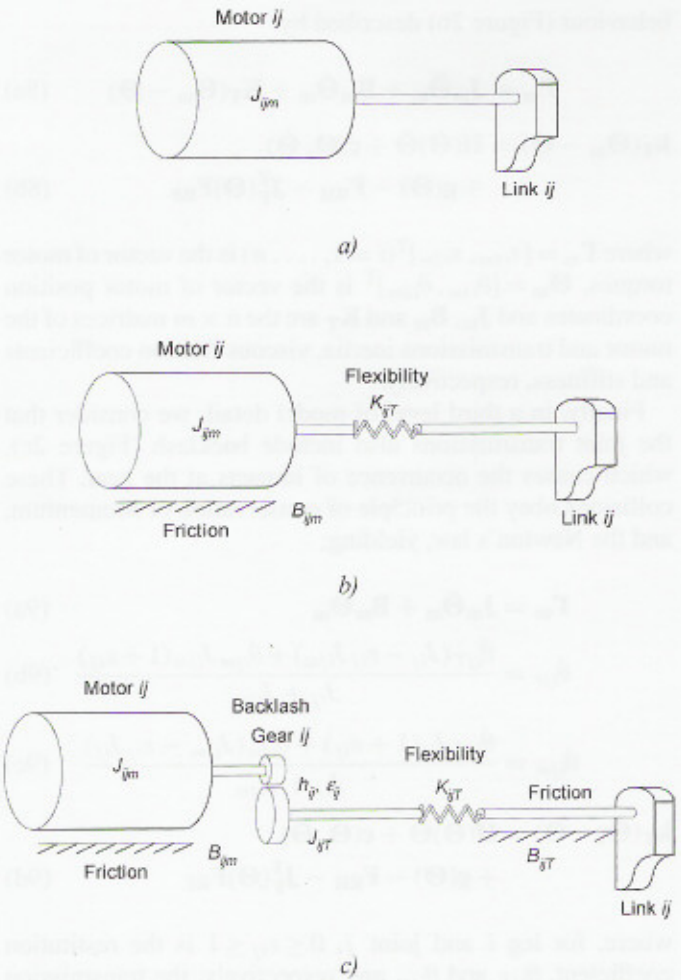

Fig. 2. Model of the leg joint: *a*) ideal actuator and transmission, *b*) actuator with friction and transmission flexibility, and *c*) actuator and transmission with friction, flexibility and backlash.

$\mathbf{F_{RF}}$ is the $m \times 1$ vector of the reaction forces that the ground exerts on the robot feet. Consequently, the $\mathbf{F_{RF}}$ forces are null during the foot transfer phase. During the system simulation, equation (6) is integrated numerically through the Runge-Kutta two method.

III.2. Dynamical effects at the joints

Furthermore, we consider that the joint actuators are not ideal, exhibiting a saturation given by:

$$\tau_{ijm} = \begin{cases} \tau_{ijC}, & |\tau_{ijm}| \leq \tau_{ijMax} \\ \mathrm{sgn}(\tau_{ijC})\tau_{ijMax}, & |\tau_{ijm}| > \tau_{ijMax} \end{cases} \tag{7}$$

where, for leg i and joint j, τ_{ijC} is the controller demanded torque, τ_{ijMax} is the maximum torque that the actuator can supply and τ_{ijm} is the motor effective torque.

The simulation also supports different dynamical effects at the joints implemented through distinct model levels of detail.

In a first level of modelling, we consider that the joint actuators and transmissions are ideal (Figure 2a). Afterwards, in a second level of detail, we consider that the joint transmissions are non-ideal, exhibiting a compliant

behaviour (Figure 2b) described by:

$$\boldsymbol{\Gamma}_{\mathbf{m}} = \mathbf{J}_{\mathbf{m}}\ddot{\boldsymbol{\Theta}}_{\mathbf{m}} + \mathbf{B}_{\mathbf{m}}\dot{\boldsymbol{\Theta}}_{\mathbf{m}} + \mathbf{K}_{\mathbf{T}}(\boldsymbol{\Theta}_{\mathbf{m}} - \boldsymbol{\Theta}) \quad (8a)$$

$$\mathbf{k}_{\mathbf{T}}(\boldsymbol{\Theta}_{\mathbf{m}} - \boldsymbol{\Theta}) = \mathbf{H}(\boldsymbol{\Theta})\ddot{\boldsymbol{\Theta}} + \mathbf{c}(\boldsymbol{\Theta}, \dot{\boldsymbol{\Theta}}) + \mathbf{g}(\boldsymbol{\Theta}) - \mathbf{F}_{\mathbf{RH}} - \mathbf{J}_{\mathbf{F}}^{\mathrm{T}}(\boldsymbol{\Theta})\mathbf{F}_{\mathbf{RF}} \quad (8b)$$

where $\boldsymbol{\Gamma}_{\mathrm{m}} = [\tau_{i1m}, \tau_{i2m}]^{\mathrm{T}} (i = 1, \ldots, n)$ is the vector of motor torques, $\boldsymbol{\Theta}_{\mathbf{m}} = [\theta_{i1m}, \theta_{i2m}]^{\mathrm{T}}$ is the vector of motor position coordinates and $\mathbf{J}_{\mathbf{m}}$, $\mathbf{B}_{\mathbf{m}}$ and $\mathbf{K}_{\mathbf{T}}$ are the $n \times m$ matrices of the motor and transmissions inertia, viscous friction coefficients and stiffness, respectively.

Finally, in a third level of model detail, we consider that the joint transmissions also include backlash (Figure 2c), which causes the occurrence of impacts at the gear. These collisions obey the principle of conservation of Momentum, and the Newton's law, yielding:

$$\boldsymbol{\Gamma}_{\mathbf{m}} = \mathbf{J}_{\mathbf{m}}\ddot{\boldsymbol{\Theta}}_{\mathbf{m}} + \mathbf{B}_{\mathbf{m}}\dot{\boldsymbol{\Theta}}_{\mathbf{m}} \quad (9a)$$

$$\dot{\theta}_{ijT} = \frac{\dot{\theta}_{ijT}(J_{ij} - \varepsilon_{ij}J_{ijm}) + \dot{\theta}_{ijm}J_{ijm}(1 + \varepsilon_{ij})}{J_{ij} + J_{ijm}} \quad (9b)$$

$$\dot{\theta}_{ijm} = \frac{\dot{\theta}_{ijT}J_{ij}(1 + \varepsilon_{ij}) + \dot{\theta}_{ijm}(J_{ijm} - \varepsilon_{ij}J_{ij})}{J_{ij} + J_{ijm}} \quad (9c)$$

$$\mathbf{k}_{\mathbf{T}}(\boldsymbol{\Theta}_{\mathbf{T}} - \boldsymbol{\Theta}) = \mathbf{H}(\boldsymbol{\Theta})\ddot{\boldsymbol{\Theta}} + \mathbf{c}(\boldsymbol{\Theta}, \dot{\boldsymbol{\Theta}}) + \mathbf{g}(\boldsymbol{\Theta}) - \mathbf{F}_{\mathbf{RH}} - \mathbf{J}_{\mathbf{F}}^{\mathrm{T}}(\boldsymbol{\Theta})\mathbf{F}_{\mathbf{RF}} \quad (9d)$$

where, for leg i and joint j, $0 \leq \varepsilon_{ij} \leq 1$ is the restitution coefficient, θ_{ijT} and θ_{ijm} are, respectively, the transmission and motor position coordinates just before the impact and θ'_{ijT} and θ'_{ijm} are the corresponding position coordinates just after the impact, J_{ij} and J_{ijm} are the leg link and motor inertia, respectively, and $\boldsymbol{\Theta}_{\mathbf{T}} = [\theta_{i1T}, \theta_{i2T}]^{\mathrm{T}}$ is the vector of transmission position coordinates.

III.3. Robot body model

Figure 1 presents the dynamic model for the hexapod body and foot-ground interaction.

This was considered a robot body compliance because walking animals have a spine that allows supporting the locomotion with improved stability.[45] This model is inspired on several studies that point out this structure. For example, the hedgehog presents muscles in the omoplata that apparently actuate as spring dashpot systems. This biomechanical structure absorbs part of the energy generated during the feet contact with the ground and returns that energy a little before the feet lift-off the ground.[25]

In fact, several authors have also followed this line of thought. Some walking robots adopt a structure similar to a spine having, however, a smaller number of *dof* than the animals in which they are inspired.[46] Berkemeier proposed a quadruped model having a body-leg connection implemented through a linear spring-dashpot system.[47] This model seems to agree with biomechanics, since it is recognized that animals use the compliance of muscles and tendons in order to increase their locomotion efficiency.[48] Therefore, the joint actuators are placed in series with the spring-dashpot system, just like in the case of animals where the muscles are in series with the tendons. The quadruped robot of Zhifeng *et al.* uses a passive spring actuated degree of freedom at the hip joint in order to accommodate to ground irregularities.[49]

Table I. System parameters.

Robot model parameters			
S_P	1 m	L_{lj}	0.5 m
O_i	0 m	M_b	88.0 kg
M_{lj}	1 kg	M_{lf}	0.1 kg
K_{xH}	10^5 Nm^{-1}	K_{yH}	10^4 Nm^{-1}
B_{xH}	10^3 Nsm^{-1}	B_{yH}	10^2 Nsm^{-1}
J_{l1m}	0.00375 kgm^2	J_{l2m}	0.000625 kgm^2
B_{ljm}	10 Nm rad^{-1}s	K_{ljT}	100000 Nm rad^{-1}
B_{ljT}	10 Nm rad^{-1}s	h_{lj}	0.001 rad
ε_{lj}	0.8	J_{l1T}	0.001875 kgm^2
J_{l2T}	0.0003125 kgm^2		
Locomotion parameters		Ground parameters	
β	50%	K_{xF}	1302152.0 Nm^{-1}
L_S	1 m	K_{yF}	1705199.0 Nm^{-1}
H_B	0.9 m	B'_{xF}	2364932.0 Nsm^{-1}
F_C	0.1 m	B'_{yF}	2706233.0 Nsm^{-1}
V_F	1 ms^{-1}	v_y	0.9

In the present study, the robot body is divided in n identical segments (each with mass $M_b n^{-1}$) and a linear spring-dashpot system is adopted to implement the intra-body compliance:

$$f_{ixH} = \sum_{i'=1}^{u}[-K_{xH}(x_{iH} - x_{i'H}) - B_{xH}(\dot{x}_{iH} - \dot{x}_{i'H})] \quad (10a)$$

$$f_{iyH} = \sum_{i'=1}^{u}[-K_{yH}(y_{iH} - y_{i'H}) - B_{yH}(\dot{y}_{iH} - \dot{y}_{i'H})] \quad (10b)$$

where $(x_{i'H}, y_{i'H})$ are the hip coordinates and u is the total number of segments adjacent to leg i, respectively.

Concerning the definition of the numerical values for the parameters of (10a) and (10b) different methods have been proposed. Bhat presents a model of a human being where the distinct body segments are joined through linear spring-dashpot systems.[50] The set of parameter values for these systems are identified from tests on human beings. On the other hand, Villanova *et al.* propose that the parameters of the passive joints of a hedgehog model, implemented through linear spring-dashpot systems, should be such that the simulated trajectories are similar to the real ones.[25] In this study, the parameters $B_{\eta H}$ and $K_{\eta H}$ ($\eta = \{x, y\}$) are defined so that the body behaviour is similar to the one expected to occur on a live animal (Table I).

IV. FOOT-GROUND INTERACTION MODEL

The contact of the robot feet with the ground can be analyzed through different viewpoints leading to distinct models. One method is to use the exact force-deflection relationships. Another method, and under specific restrictions, is to use approximate models of the ground deformation based on the studies of soil mechanics.

One example of the first approach was used by Manko, which models the foot-ground interactions through force-deflection relationships, for different loading conditions on flat and sloped surfaces.[1] Manko uses a bilinear equation for the vertical foot-ground interactions while the lateral forces are modelled with an expression describing an exponential transition to Coulomb's equation. Another example was given by Bekker that relates the vertical sinkage and the local pressure normal to the ground surface through an exponential function.[51] Bekker relates the horizontal deflection with the local shear stress at the ground surface using a ratio of exponential functions.

The second approach models the foot-ground interaction through a linear system with damping $B_{\eta F}$ and stiffness $K_{\eta F}(\eta = \{x, y\})$ in the {horizontal, vertical} directions, respectively, according to equation:[52]

$$f_{i\eta F} = -K_{\eta F}(\eta_{iF} - \eta_{iF0}) - B_{\eta F}(\dot{\eta}_{iF} - \dot{\eta}_{iF0}) \qquad (11)$$

where η_{iF0} are the coordinates of foot i touchdown.

This point of view was used by several authors. For example, Lee *et al.* study a quadruped using a linear spring-dashpot system to simulate the ground behaviour.[53] They adopt numerical values for the parameters so that the forces at the robot feet are identical to the pseudo-inverse solution for the same model considering closed kinematic chains. Taga has a similar model for the ground but adopts identical values for the parameters independently of the force direction ($K_{\eta F} = 30000.0\,\mathrm{Nm}^{-1}$ and $B_{\eta F} = 1000.0\,\mathrm{Nsm}^{-1}$).[54]

Another approach, used in the present article, estimates the values for the parameters based on the studies of soil mechanics. The parameters are given by $K_{xF} = 2(1+\mu)G\beta_x\sqrt{BL}$ and $K_{yF} = [G/(1-\mu)]\beta_y\sqrt{BL}$, where μ if the Poisson's ratio (that varies from 0.35, for soils of low saturation, up to 0.5, for fully saturated soils[52]), B is the width of the feet touching the ground and L the corresponding length. The values of β_x and β_y are extracted from pre-calculated tables as functions of L/B.[52] Finally, G is the shear modulus and is calculated using the expression $G = E/[2(1+\mu)]$ where E if the Young's modulus of elasticity of the soil type. The Young's modulus of elasticity of some common soil types are indicated in Table II.[55]

Concerning the values of damping (B_{xF} and B_{yF}) these can be calculated considering that the above expressions apply to a mass-spring-dashpot system whose damping ratios are extracted from pre-calculated tables as functions of $b = M/(\rho R^3)$ where M if the equivalent mass of the system under consideration (in our case $M_b n^{-1}$), ρ is the soil mass density and R is the radius of the feet-ground contact area.[52,55] For the typical dimensions of the robot under consideration, the ground damping ratio both in the horizontal and vertical directions is $\zeta < 0.15$.

Based on the above equations, Table II presents the values for the ground model parameters of typical soils commonly found in nature and in the living environments.

While computationally simple, the linear foot-ground interaction model presents several weaknesses.[56] The first inconsistency is that the contact force is discontinuous at the moment of impact. The second problem is that the model allows not only forces due to compression at the contact point but also forces that tend to hold the objects together. A final weakness is the dependence of the coefficient of restitution on the mass of the impacting bodies and the lack of dependence on the impact velocity. A solution to these shortcomings, proposed by Hunt and Crossley, is to replace the linear spring/damper parallel combination through a non-linear one.[57]

While Hunt and Crossley make use of non-linear stiffness and friction elements,[57] we adopt a mixed strategy, that is, we model the contact of the ith robot feet with the ground through a linear stiffness $K_{\eta F}$ and a non-linear damping $B'_{\eta F}(\eta = \{x, y\})$ in the {horizontal, vertical} directions, respectively, yielding:

$$\begin{aligned} f_{i\eta F} &= -K_{\eta F}(\eta_{iF} - \eta_{iF0}) \\ &\quad - B'_{\eta F}[-(y_{iF} - y_{iF0})]^{v_\eta}(\dot{\eta}_{iF} - \dot{\eta}_{iF0}), \\ v_x &= 1.0,\ v_y = 0.9 \end{aligned} \qquad (12)$$

where x_{iF0} and y_{iF0} are the coordinates of foot i touchdown and v_η is a parameter dependent on the ground characteristics.[57]

In order to convert the parameters of this non-linear foot-ground interaction model (B'_{xF}, B'_{yF}) to the parameters of the linear model (B_{xF}, B_{yF}), described by equation (11), we use the following relations:

$$-B'_{\eta F}(-\Delta_{iyFMax})^{v_\eta} = -B_{\eta F} \qquad (13)$$

where Δ_{iyFMax} if the maximum depth that the robot feet penetrates the ground.

V. MODEL TEST

In this section we present a set of experiments to evaluate the system modelling for a hexapod locomotion adopting

Table II. Young's moduli and ground model parameters for different soil types.

Soil Type	Young's Modulus (kNm^{-2})	K_{xF} (Nm^{-1})	B_{xF} (Nsm^{-1})	K_{yF} (Nm^{-1})	B_{yF} (Nsm^{-1})
Concrete	30000000	2604304130	153097	3410398265	175196
Wood	13000000	1128531790	100781	1477839248	115328
Gravel	100000–200000	17362028	12500	22735988	14305
Sand	10000–80000	6944811	7906	9094395	9047
Compact Clay	3000–15000	1302152	3423	1705199	3917
Loose Clay	500–3000	260430	1531	341040	1752
Peat	100–500	43405	625	56840	715

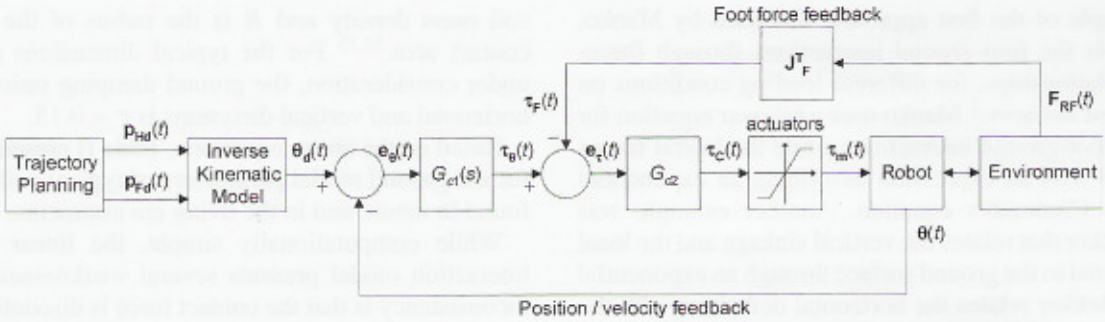

Fig. 3. Robot control architecture.

the periodic wave gait and different dynamic phenomena at the leg joints. For simulation purposes we consider the locomotion, robot and ground parameters presented in Table I.

The control algorithm adopted for the robot leg joints is introduced in the next sub-section. This controller is the basis for the stable robot locomotion. In sub-section V.2 the results of several simulations are presented in order to demonstrate the correct performance of the robot model implemented both in terms of trajectory planning, dynamics and control.

V.1. Control architecture

The general control architecture of the hexapod robot is presented in Figure 3. The trajectory planning is held at the cartesian space but the control is performed in the joint space, which requires the integration of the inverse kinematic model in the forward path. The base algorithm considers only a position/velocity feedback and, in that case, the series of $G_{c1}(s)$ and G_{c2} can be substituted by a single block. Nevertheless, the base architecture is improved with the introduction of a second internal feedback loop with information of the foot-ground interaction force. In the case of force feedback, $G_{c1}(s)$ and G_{c2} form a cascade structure in the forward control path. The superior performance of introducing force feedback was highlighted for the case of having non-ideal actuators with saturation or variable ground characteristics.[23]

Based on these results, in this study we adopt a *FO* controller for $G_{c1}(s)$ and a simple *P* controller for G_{c2}. The *FO* algorithm consists on:

$$G_{C1j}(s) = K_{pj} + K_{\alpha j} s^{\alpha j}, \quad \alpha_j \in \mathbb{R}, \quad j = 1, 2 \qquad (14)$$

where K_{pj} and $K_{\alpha j}$ are the proportional and derivative gains, respectively, and α_j is the fractional order.

In what concerns equation (14) it should be noted that the mathematical definition of a derivative of fractional order has been the subject of several different approaches.[58] For example, (15a) and (15b), represent the Laplace (for zero initial conditions) and the Grünwald-Letnikov definitions of the fractional derivative of order α of the signal $x(t)$:

$$D^\alpha[x(t)] = L^{-1}\{s^\alpha X(s)\} \qquad (15a)$$

$$D^\alpha[x(t)] = \lim_{h\to 0}\left[\frac{1}{h^\alpha}\sum_{k=1}^{\infty}\frac{(-1)^k\Gamma(\alpha+1)}{\Gamma(k+1)\Gamma(\alpha-k+1)}x(t-kh)\right] \qquad (15b)$$

where Γ is the gamma function and h is the time increment.

Table III. Padé approximation coefficients.

a_{ij0}	1.000000000	b_{ij0}	1.000000000
a_{ij1}	−2.250000000	b_{ij1}	−1.750000000
a_{ij2}	1.687500000	b_{ij2}	0.937500000
a_{ij3}	−0.468750000	b_{ij3}	−0.156250000
a_{ij4}	0.035156250	b_{ij4}	0.003906250

Table IV. Controller parameters.

	Joint $j=1$		Joint $j=2$
K_{p1}	1500	K_{p2}	4000
$K_{\alpha 1}$	300	$K_{\alpha 2}$	10
α_1	0.5	α_2	0.5

In this paper, for implementing the *FO* algorithm (14) it is adopted a discrete-time 4th-order Padé approximation (a_{ijk}, $b_{ijk} \in \Re$, $j = 1, 2$) yielding an equation in the z-domain of the type:

$$G_{C1j}(z) \approx K_j \sum_{k=0}^{k=4} a_{ijk} z^{-k} \Big/ \sum_{k=0}^{k=4} b_{ijk} z^{-k} \qquad (16)$$

where K_j is the controller gain and the coefficients of the Padé approximation are presented in Table III.

The discrete-time control algorithm is evaluated with a sampling frequency of $f_{sc} = 2.0\,\text{kHz}$ while the robot and environment are simulated with a sampling frequency of $f_{sr} = 20.0\,\text{kHz}$.

To tune the controller parameters we adopt a systematic method, testing and evaluating several possible combinations of controller parameters. Moreover, it is assumed high performance joint actuators with a maximum actuator torque in (7) of $\tau_{ijMax} = 400\,\text{Nm}$. The adopted controller parameters are presented in Table IV.

V.2. Simulation results

With the system and controller parameters established previously, in this section we analyse the simulation model.

For example, Figures 4 and 5 present the charts of the planned foot position, velocity and acceleration in the operational space for the *WG*, with $\beta = 50\%$, and the *EPFCG*, with $\beta = 35\%$, respectively. It is possible to observe that in the second situation the robot can achieve the same foot trajectory with lower values of velocity and acceleration, because the transference time (t_T) is superior. The corresponding

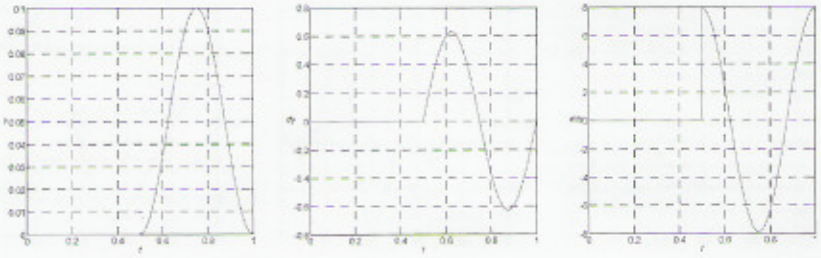

Fig. 4. Planned cartesian coordinates: position $y_{1F}(t)$, velocity $\dot{y}_{1F}(t)$ and acceleration $\ddot{y}_{1F}(t)$, for the *WG* and $\beta = 50\%$.

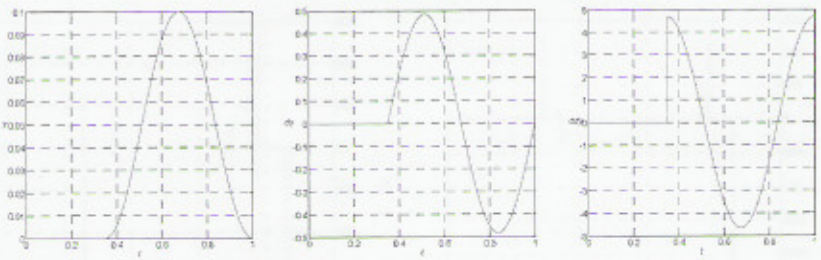

Fig. 5. Planned Cartesian coordinates: position $y_{1F}(t)$, velocity $\dot{y}_{1F}(t)$ and acceleration $\ddot{y}_{1F}(t)$, for the *EPFCG* and $\beta = 35\%$.

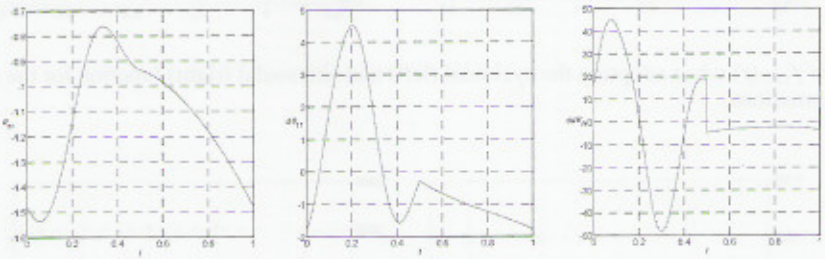

Fig. 6. Planned joint coordinates: position $\theta_{11}(t)$, velocity $\dot{\theta}_{11}(t)$ and acceleration $\ddot{\theta}_{11}(t)$, for the *WG* and $\beta = 50\%$.

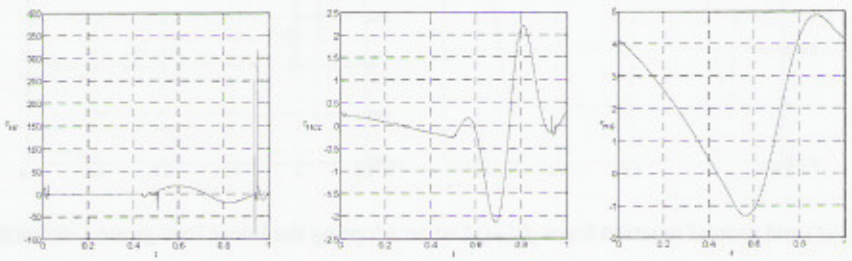

Fig. 7. Leg 1 hip joint torque terms: inertial $\tau_{11I}(t)$, centrifugal/Coriolis $\tau_{11CC}(t)$ and gravitational $\tau_{11G}(t)$, for the *WG* and $\beta = 50\%$.

coordinates in the joint space, for the case of the *WG*, are presented in Figure 6.

Once established the trajectory planning and the kinematics the simulation requires the dynamics and the control algorithms. We consider, for example, that the robot leg joints are controlled through the *FO* algorithm with the parameters presented in Table IV. The resulting robot model joint torques are analysed for the above two locomotion examples. Figures 7 and 8 depict the corresponding inertial, centrifugal/Coriolis and gravitational torque terms at the hip joint of leg 1. Comparing the robot locomotion on both situations, it is possible to observe that the inertial component of the torque is higher for the case of the *WG* with $\beta = 50\%$. This reflects the fact that the feet trajectory must be accomplished in a shorter time interval, as previously mentioned, leading to higher accelerations and, therefore, to a larger inertial torque component. Moreover, in this case we have higher velocities leading also to higher centrifugal/Coriolis torque components as can be observed by comparing Figures 7 and 8. Finally, and since the robot planned feet trajectory is equal on both cases, the gravitational component of the joint torque is similar for the two situations under evaluation.

It is worth notice the large amplitude spikes observed in the charts of the inertial component of the torque, and of smaller amplitude in the centrifugal/Coriolis torque component, around $t = 0.9$ s. These are due to the large forces that originate during the feet impact with the ground, giving rise to torques that propagate through the leg mechanical structure up to the joints.

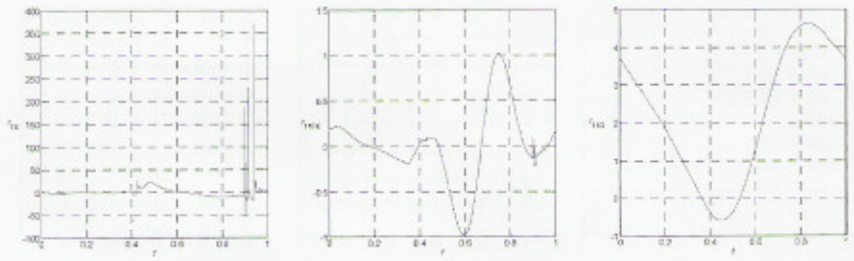

Fig. 8. Leg 1 hip joint torque terms: inertial $\tau_{11I}(t)$, centrifugal/Coriolis $\tau_{11CC}(t)$ and gravitational $\tau_{11G}(t)$, for the *EPFCG* and $\beta = 35\%$.

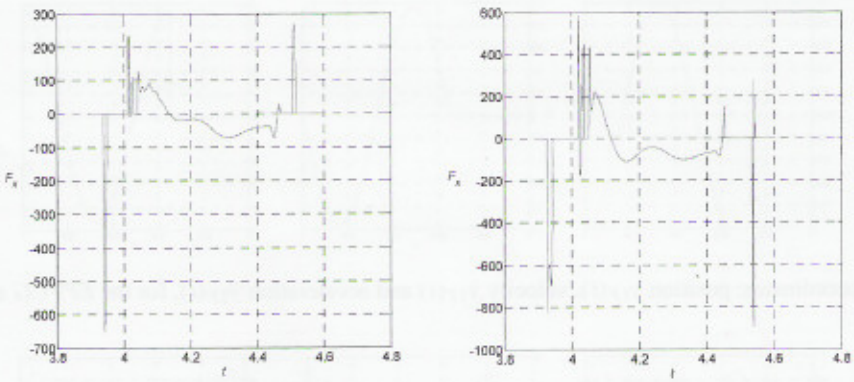

Fig. 9. Ground reaction force $f_{1xF}(t)$ when adopting the cycloidal (left) and sinusoidal (right) function for the feet reference trajectory and a robot with ideal joint transmissions.

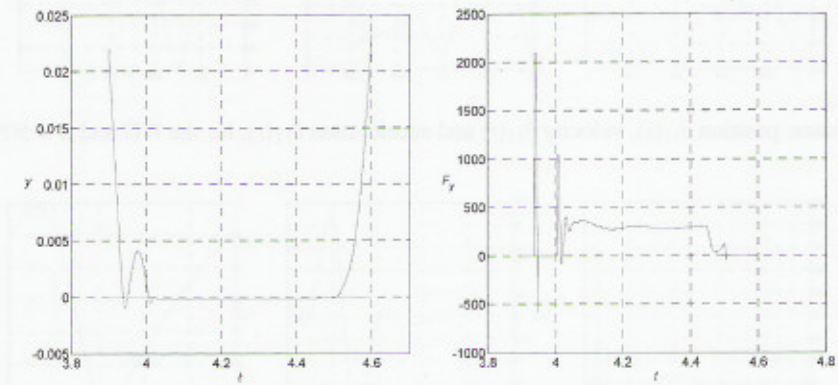

Fig. 10. Foot coordinate $y_{1F}(t)$ and ground reaction force $f_{1yF}(t)$ when adopting the linear foot-ground interaction model and a robot with ideal joint transmission.

The next step is the comparison of the robot locomotion while adopting the cycloidal (1a) and the sinusoidal function (1b) for the feet transfer phase trajectory. For this purpose, an analysis of the ground reaction forces, at the instants of feet touch-down and lift-off, is presented. We start by simulating the robot walking with the *WG* and $\beta = 50\%$, while adopting a cycloidal feet trajectory and, in a second experiment we consider the case of a sinusoidal feet trajectory.

Figure 9 presents the charts of the ground reaction force f_{1xF} for both feet trajectories. It is noticeable that the sinusoidal feet trajectories impose higher values for the feet reaction forces, particularly at the instants of feet landing and take-off, in agreement with the conclusions presented in section II.2.

We can also analyse the foot-ground interaction and compare the linear *versus* the non-linear spring-dashpot models. Figures 10 and 11 present charts of the foot coordinate $y_{1F}(t)$ and the ground reaction force $f_{1yF}(t)$ for both cases. We conclude that $y_{1F}(t)$ is similar for the two models but the charts of $f_{1yF}(t)$ present significant differences. We observe that in case of the linear model $f_{1yF}(t)$ presents negative values for this force, meaning that the ground is pulling the feet which, in general, is not reasonable. Although not visible on these plots, for the linear foot-ground interaction model the force $f_{1yF}(t)$ presents an instantaneous discontinuity to the maximum value, when the foot contacts the ground. Both these situations disappear if we adopt the non-linear model, as previously referred in section IV.

The above experiments where performed assuming ideal robot joint transmissions and high performance joint actuators with a maximum actuator torque in (7) of

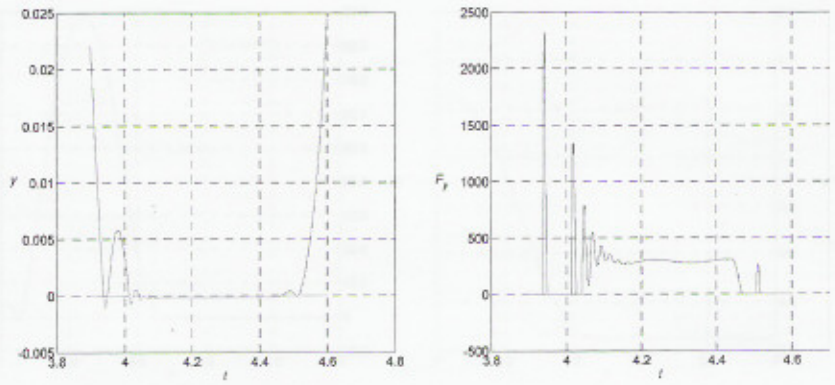

Fig. 11. Foot coordinate $y_{1F}(t)$ and ground reaction force $f_{1yF}(t)$ when adopting the non-linear foot-ground interaction model and a robot with ideal joint transmission.

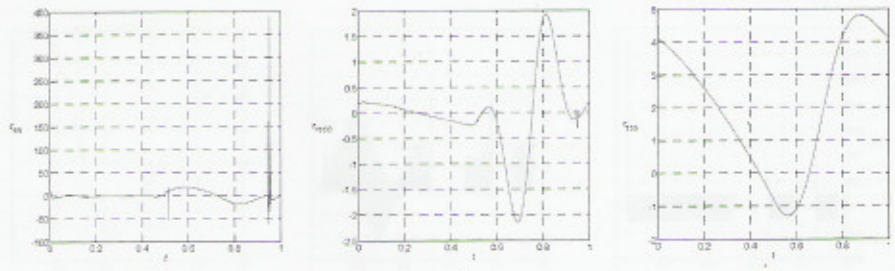

Fig. 12. Leg 1 hip joint torque terms: inertial $\tau_{11I}(t)$, centrifugal/Coriolis $\tau_{11CC}(t)$ and gravitational $\tau_{11G}(t)$, for the *WG* and $\beta = 50\%$. Robot with joint transmissions having friction and flexibility.

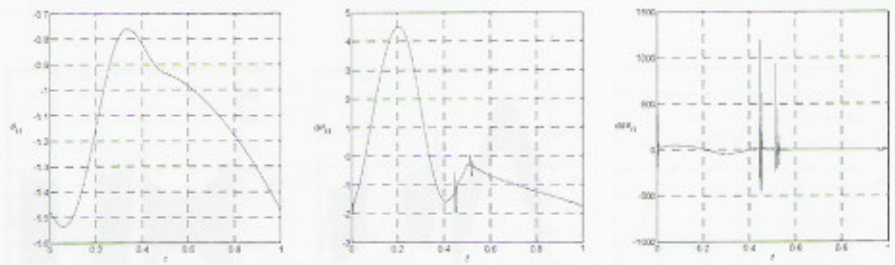

Fig. 13. Resulting joint coordinates: position $\theta_{11}(t)$, velocity $\dot{\theta}_{11}(t)$ and acceleration $\ddot{\theta}_{11}(t)$, for the *WG* and $\beta = 50\%$. Robot with joint transmissions having friction and flexibility.

$\tau_{ijMax} = 400\,\text{Nm}$. In the next experiments we verify the effect of joint transmissions having friction, flexibility and backlash, while maintaining the actuators saturation characteristics and a robot walking with the *WG* and $\beta = 50\%$.

Figure 12 presents the charts of the inertial, centrifugal/Coriolis and gravitational torque terms applied at the hip joint of leg 1, for the case of joint transmissions having friction and flexibility. Comparing the charts of Figures 12 and 13 with those of Figures 7 and 6, respectively, we conclude that they are almost similar. As previously observed the charts of the inertial and centrifugal/Coriolis terms of the torques and of the real velocity and acceleration, present large amplitude spikes at the instants of feet landing.

The corresponding foot trajectory in the cartesian space is presented in Figure 14. It is clearly seen that this trajectory is quite smooth. It is also possible to observe a small rebounce on the $y_{1F}(t)$ foot trajectory that occurs after the feet touch the ground, at $t \approx 0.95$ s.

The last experiment considers that the robot joint transmissions have not only friction and flexibility but also backlash. The effect of joint transmissions having backlash is clearly seen in some of the charts of Figures 15 and 16, namely in the inertial torque terms and in the joint acceleration, respectively. These charts present a visible chattering, due to the multiple impacts that occur at the gear. The corresponding cartesian foot trajectory is presented in Figure 17. Comparing the charts of Figure 17 and Figure 14, it is clear a degradation of the foot trajectory following and the occurrence of several rebounces.

From the result analysis of the previous experiments, we conclude that the robot simulation model, described in this paper, implements correctly the planning, kinematic, dynamic and control schemes, for the locomotion of the hexapod, allowing the simulation of different walking gaits. Moreover, the behaviour observed while the feet contact the ground seems to represent faithfully the real system.

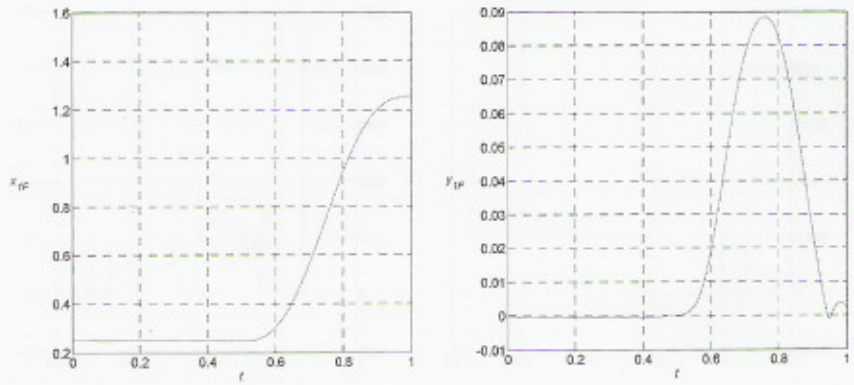

Fig. 14. Cartesian foot position $x_{1F}(t)$ and $y_{1F}(t)$, for the *WG* and $\beta = 50\%$. Robot with joint transmissions having friction and flexibility.

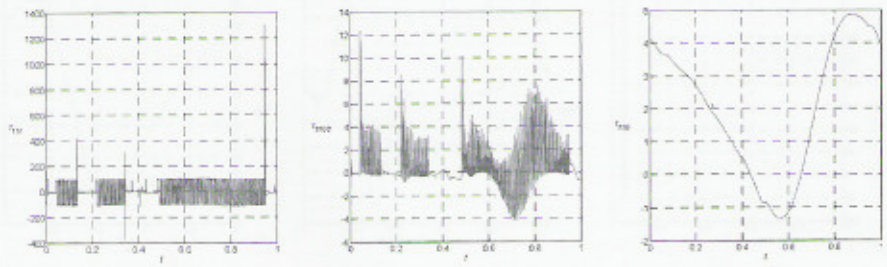

Fig. 15. Leg 1 hip joint torque terms: inertial $\tau_{11I}(t)$, centrifugal/Coriolis $\tau_{11CC}(t)$ and gravitational $\tau_{11G}(t)$, for the *WG* and $\beta = 50\%$. Robot with joint transmissions having friction, flexibility and backlash.

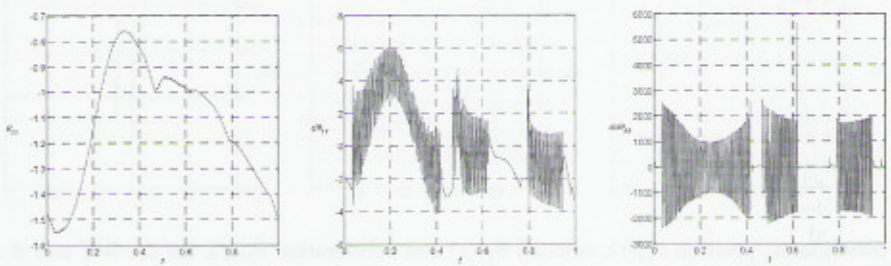

Fig. 16. Resulting joint coordinates: position $\theta_{11}(t)$, velocity $\dot{\theta}_{11}(t)$ and acceleration $\ddot{\theta}_{11}(t)$, for the *WG* and $\beta = 50\%$. Robot with joint transmissions having friction, flexibility and backlash.

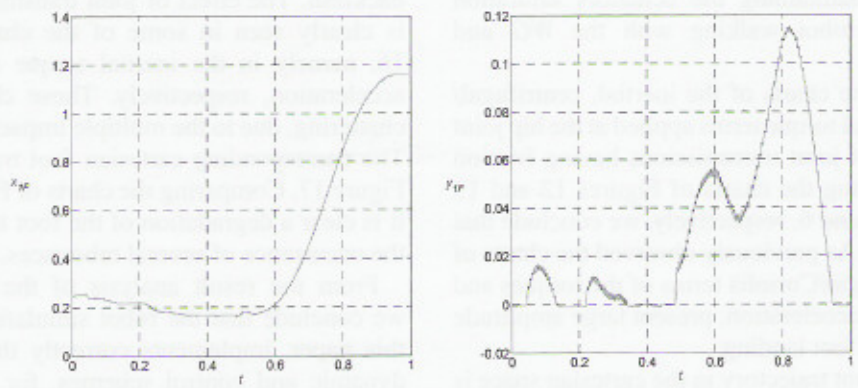

Fig. 17. Cartesian foot position $x_{1F}(t)$ and $y_{1F}(t)$, for the *WG* and $\beta = 50\%$. Robot with joint transmissions having friction, flexibility and backlash.

VI. CONCLUSIONS

In this paper we have presented a simulation model for multi-legged locomotion systems with segmented body. This tool is the basis for the study of the best system configuration and the type of movements that lead to a better mechanical implementation and for joint leg control algorithm testing.

The walking robot model includes the trajectory planning, for several different periodic walking gaits, the kinematics and the dynamics. Furthermore, the robot foot-ground interactions are also considered.

By implementing joint leg actuators and transmission models that incorporate dynamical phenomena, such as a non-ideal saturation, viscous friction, backlash and flexibility, we are able to estimate how the robot controllers responds to a degradation of the actuators characteristics. In this paper, for the simulation evaluation it was adopted a *FO* joint controller algorithm.

The results are compatible with the engineering practice and experimental knowledge demonstrating the correctness of the algorithms and parameters adopted in the modelling and simulation.

References

1. D. J. A. Manko, *A General Model of Legged Locomotion on Natural Terrain* (Kluwer. Westinghouse Electric Corporation, 1992).
2. S.-M. Song and K. J. Waldron, *Machines that Walk: The Adaptive Suspension Vehicle* (The MIT Press. 1989).
3. S. Bai, K. H. Low and T. Zielinska, "Quadruped Free Gait Generation for Straight-Line and Circular Trajectories," *Adv. Rob.* **13**, 513–538 (1999).
4. K. Inagaki, "A Gait Study for a One-Leg-Disabled Hexapod Robot," *Adv. Rob.* **12**, 593–604 (1999).
5. D. W. Marhefka and D. E. Orin, "Gait Planning for Energy Efficiency in Walking Machines," *Proc. IEEE Int. Conf. on Rob. & Aut.* (1997) pp. 474–480.
6. C.-H. Chen, V. Kumar and Y.-C. Luo, "Motion Planning of Walking Robots Using Ordinal Optimization," *IEEE Rob. & Aut. Magazine* **5**, 22–32 (1998).
7. D. J. Cho, J. H. Kim and D. G. Gweon, "Optimal Turning Gait of a Quadruped Walking Robot," *Robotica* **13**(4), 559–564 (1995).
8. S. Bai, K. H. Low and M. Y. Teo, "Path Generation of Walking Machines in 3D Terrain," *Proc. IEEE Int. Conf. on Rob. & Aut.* 2216–2221 (2002).
9. T. McGeer, "Passive Dynamic Walking," *Int. J. of Rob. Res.* **9**, 62–82 (1990).
10. A. C. Smith and M. D. Berkemeier, "Passive Dynamic Quadrupedal Walking," *Proc. IEEE Int. Conf. on Rob. & Aut.* (1997) pp. 34–39.
11. M. C. Birch, R. D. Quinn, G. Hahm, S. M. Phillips, B. Drennan, A. Fife, H. Verma and R. D. Beer, "Design of a Cricket Microrobot," *Proc. IEEE Int. Conf. on Rob. & Aut.* (2000) pp. 1109–1114.
12. C.-R. Tsai, T.-T. Lee and S.-M. Song, "Fuzzy Logic Control of a Planetary Gear Type Walking Machine Leg," *Robotica* **15**(4), 533–546 (1997).
13. J. J. Collins and S. A. Richmond, "Hard-Wired Central Pattern Generators for Quadrupedal Locomotion," *Biological Cybernetics* **71**, 375–385 (1994).
14. D. Wettergreen, "Robotic Walking in Natural Terrain – Gait Planning and Behavior-Based Control for Statically-Stable Walking Robots," *PhD. Thesis* (The Robotics Institute, Carnegie Mellon University, 1995).
15. A. Torres, "Virtual Model Control of a Hexapod Walking Robot," *BSc. Thesis* (Department of Mechanical Engineering, Massachusetts Institute of Technology, 1996).
16. L. de S. Martins-Filho, J. L. Silvino, P. Resende and T. C. Assunção, "Control of Robotic Leg Joints – Comparing PD and Sliding Mode Approaches," *Proc. CLAWAR'2003 – 6th Int. Conf. on Climbing and Walking Robots* (2003) pp. 147–153.
17. K.-P. Lee, T.-W. Koo and Y.-S. Yoon, "Real-Time Dynamic Simulation of Quadruped Using Modified Velocity Transformation," *Proc. IEEE Int. Conf. on Rob. & Aut.* (1998) pp. 1701–1706.
18. J. Song, K. H. Low and W. Guo, "A Simplified Hybrid Force/Position Controller Method for the Walking Robots," *Robotica* **17**(4), 583–589 (1999).
19. M. F. Silva, J. A. T. Machado and A. M. Lopes, "Power Analysis of Multi-Legged Locomotion Systems," *Proc. CLAWAR'2001 – 4th Int. Symposium on Climbing and Walking Robots* (2001) pp. 143–150.
20. M. F. Silva, J. A. T. Machado and A. M. Lopes, "Performance Analysis of Multi-Legged Locomotion Systems," *Proc. IEEE Int. Conf. on Rob. & Aut.* (2002) pp. 2234–2239.
21. M. F. Silva, J. A. T. Machado and A. M. Lopes, "Power Analysis of Multi-Legged Systems," *Proc. b'02 – 15th IFAC World Congress on Automatic Control* (In CD-ROM) (2002).
22. M. F. Silva, J. A. T. Machado and A. M. Lopes, "Cascade Control of a Hexapod Robot," *Proc. CLAWAR'2003 – 6th Int. Conf. on Climbing and Walking Robots* (2003) pp. 163–170.
23. M. F. Silva, J. A. T. Machado and A. M. Lopes, "Position / Force Control of a Walking Robot," *MIROC – Machine Intelligence and Robotic Control* **5**, 33–44 (2003).
24. S. Bai, K. H. Low and W. Guo, "Kinematographic Experiments on Leg Movements and Body Trajectories of Cockroach Walking on Different Terrain," *Proc. IEEE Int. Conf. on Rob. & Aut.* (2000) pp. 2605–2610.
25. J. Villanova, J.-C. Guinot, P. Neveu and J.-P. Gasc, "Quadrupedal Mammal Locomotion Dynamics 2D Model," *Proc. IEEE/RSJ Int. Conf. on Int. Rob. and Syst.* (2000) pp. 1785–1790.
26. S. Laksanacharoen, A. J. Pollack, G. M. Nelson, R. D. Quinn and R. E. Ritzmann, "Biomechanics and Simulation of Cricket for Microrobot Design," *Proc. IEEE Int. Conf. on Rob. & Aut.* (2000) pp. 1088–1094.
27. F. Pfeiffer, J. Eltze and H. Weidemann, "The TUM Walking Machine," *Intelligent Aut. and Soft Computing* **1**, 307–323 (1995).
28. K.-Y. Tu, T.-T. Lee, C.-H. Wang and C.-A. Chang, "Design of Fuzzy Walking Pattern (FWP) for a Shape Memory Alloy (SMA) Biped Robot," *Proc. IEEE Int. Conf. on Syst., Man and Cyb.* (1998) pp. 3266–3271.
29. G. M. Nelson, R. D. Quinn, R. J. Bachmann, W. C. Flannigan, R. E. Ritzmann and J. T. Watson, "Design and Simulation of a Cockroach-Like Hexapod Robot," *Proc. IEEE Int. Conf. on Rob. & Aut.* (1997) pp. 1106–1111.
30. D. C. De Campos, C. A. D. Bezerra, D. E. Zampieri and A. Mendeleck, "Modelagem e Simulação Dinâmica de um Robô Bípede," *Proc. COBEM 2001 – XVI Congresso Brasileiro de Engenharia Mecânica* (2001) pp. 92–99.
31. N. Koyachi, H. Adachi, T. Nakamura and E. Nakano, "Stair-Climbing Control of Self-Contained Hexapod With Semi-Fixed Gait," *Proc. IEEE Int. Conf. on Adv. Rob.* (1991) pp. 747–752.
32. C. Queiroz, N. Gonçalves and P. Menezes, "A Study on Static Gaits for a Four Leg Robot," *Proc. CONTROL 2000 – UK ACC Int. Conf. on Control* (In CD-ROM) (2000).
33. N. Koyachi, T. Arai, H. Adachi, A. Murakami and K. Kawai, "Mechanical Design of Hexapods With Integrated Limb Mechanism: MELMANTIS-1 and MELMANTIS-2," *Proc. IEEE Int. Conf. on Adv. Rob.* (1997) pp. 273–278.
34. F. E. Hafi and P. Gorce, "Walking Dynamic Control Under Unknown Perturbation," *Proc. IEEE Int. Conf. on Syst., Man & Cyb.* (1998) pp. 3538–3543.

35. N. Koyachi, H. Adachi, N. Senjo, R. Murata, M. Izumi, T. Hirose and T. Arai, "Control of Walk and Manipulation by a Hexapod With Integrated Limb Mechanism: MELMANTIS-1," *Proc. IEEE Int. Conf. on Rob. & Aut.* (2002) pp. 3553–3558.
36. M. A. Jiménez and P. G. de Santos, "Terrain-Adaptive Gait for Walking Machines," *Int. J. of Rob. Research* **16**(3), 320–339 (1997).
37. S. Miossec and Y. Aoustin, "Mouvement de Marche Composé de Simple et de Double Support Pour un Robot Bipède Planaire Sans Pieds," *Proc. Conférence Int.e Francophone d'Automatique* (2002) pp. 522–527.
38. A. Muraro and C. Chevallereau, "Trajectoires Optimales Pour L'Amble d'un Quadrupède Pour des Critères Énergètiques," *Proc. Conférence Int.e Francophone d'Automatique* (2002) pp. 528–533.
39. C. Chevallereau, A. Formal'Sky and B. Perrin, "Control of a Walking Robot With Feet Following a Reference Trajectory Derived From Ballistic Motion," *Proc. IEEE Int. Conf. on Rob. & Aut.* (1997) pp. 1094–1099.
40. J. K. Hodgins, "Three-Dimensional Human Running," *Proc. IEEE Int. Conf. on Rob. & Aut.* (1996) pp. 3271–3276.
41. B. Perrin, C. Chevallereau and C. Verdier, "Calculation of the Direct Dynamic Model of Walking Robots: Comparison Between Two Methods," *Proc. Int. Conf. on Adv. Rob.* (1997) pp. 1088–1093.
42. J. P. Barreto, A. Trigo, P. Menezes, J. Dias and A. T. de Almeida, "FBD – The Free Body Diagram Method. Kinematic and Dynamic Modelling of a Six Leg Robot," *Proc. of the 5th Int. Workshop on Adv. Motion Control* (1998) pp. 423–428.
43. S. McMillan and D. E. Orin, "Forward Dynamics of Multilegged Vehicles Using the Composite Rigid Body Method," *Proc. IEEE Int. Conf. on Rob. & Aut.* (1998) pp. 464–470.
44. R. Featherstone and D. Orin, "Robot Dynamics: Equations and Algorithms," *Proc. IEEE Int. Conf. on Rob. & Aut.* (2000) pp. 826–834.
45. H. Witte, R. Hackert, M. S. Fischer, W. Ilg, J. Albiez, R. Dillmann and A. Seyfarth, "Design Criteria for the Leg of a Walking Machine Derived by Biological Inspiration from Quadrupedal Mammals," *Proc. CLAWAR'2001 – 4th Int. Conf. on Climbing and Walking Robots* (2001) pp. 63–68.
46. K. Berns, W. Ilg, M. Deck and R. Dillmann, "The Mammalian-Like Quadrupedal Walking Machine BISAM," *Proc. of the 5th Int. Workshop on Adv. Motion Control* (1998) pp. 429–433.
47. M. D. Berkemeier, "Modeling the Dynamics of Quadrupedal Running," *Int. Journal of Rob. Res.* **17**(9), 971–985 (1998).
48. R. McN. Alexander, "Three Uses for Springs in Legged Locomotion," *Int. J. of Rob. Res.* **9**(2), 53–61 (1990).
49. C. Zhifeng, Z. Xiuli, Z. Haojun and Z. Liyao, "The CPG-based Bionic Quadruped System," *Proc. IEEE Int. Conf. on Syst., Man & Cyb.* (2003) pp. 1828–1833.
50. R. B. Bhat, "Dynamic Response of Whole Body System Subjected to Walking Generated Excitation," *Proc. VIB 2003 – ASME Int. 19th Biennial Conf. on Mech. Vib. and Noise* (In CD-ROM) (2003).
51. M. G. Bekker, *Introduction to Terrain-Vehicle Systems* (University of Michigan Press. Ann Arbor, 1969).
52. T. W. Lambe and R. V. Whitman, *Soil Mechanics, SI Version* (John Wiley & Sons. 1969).
53. S. Lee, D.-S. Choi, M. Kim, C.-W. Lee and J.-B. Song, "Human and Robot Integrated Teleoperation," *Proc. IEEE Int. Conf. on Syst., Man & Cyb.* (1998) pp. 1213–1218.
54. G. Taga, "A Model of the Neuro-Musculo-Skeletal System for Human Locomotion: I. Emergence of Basic Gait," *Biological Cybernetics* **73**, 97–111 (1995).
55. A. Suvinen, M. Saarilahti and T. Tokola, "Terrain Mobility Model and Determination of Optimal Off-Road Route," *Proc. 9th Scandinavian Research Conf. on Geographical Information Science* (2003) pp. 251–259.
56. D. W. Marhefka and D. E. Orin, "Simulation of Contact Using a Nonlinear Damping Model," *Proc. IEEE Int. Conf. on Rob. & Aut.* (1996) pp. 1662–1668.
57. K. H. Hunt and F. R. E. Crossley, "Coefficient of Restitution Interpreted as Damping in Vibroimpact," *ASME J. of Applied Mechanics*, 440–445 (1975).
58. J. A. T. Machado, "Analysis and Design of Fractional-Order Digital Control Systems," *SAMS – Journal Systems Analysis-Modeling-Simulation* **27**, 107–122 (1997).